Drip Paintings and Fractal Analysis

Katherine Jones-Smith[1], Harsh Mathur[1] and Lawrence Krauss[1,2]

[1]*Department of Physics, Case Western Reserve University, 10900 Euclid Avenue, Cleveland OH 44106-7079, USA.*
[2]*Also Department of Astronomy, Case Western Reserve University.*

It has been claimed [1, 2, 3, 4, 5, 6] that fractal analysis can be applied to unambiguously characterize works of art such as the drip paintings of Jackson Pollock. This academic issue has become of more general interest following the recent discovery of a cache of disputed Pollock paintings. We definitively demonstrate here, by analyzing paintings by Pollock and others, that fractal criteria provide no information about artistic authenticity. This work has also led to two new results in fractal analysis of more general scientific significance. First, the composite of two fractals is not generally scale invariant and exhibits complex multifractal scaling in the small distance asymptotic limit. Second the statistics of box-counting and related staircases provide a new way to characterize geometry and distinguish fractals from Euclidean objects.

In 1999, a highly publicized work [2] applied fractal analysis to the works of Jackson Pollock. The recent discovery of a cache of approximately twenty-five paintings that may be the work of Pollock has motivated the application of these techniques in order to determine authenticity of these paintings. However we argued in [7] that in fact Pollock's drip-paintings cannot be usefully characterized as fractal, and that identical fractal characteristics can be trivially reproduced. In this work we analyze seven drip-paintings (three by Pollock, two of the newly discovered paintings, and two commissioned works by local artists) and demonstrate conclusively that fractal criteria are not useful for authentication. In particular, we demonstrate both that known Pollock drip-paintings, and known non-Pollock paintings meet the claimed criteria at equal levels of significance. Our detailed analysis led us to explore fractal analysis in a more general context, motivating us to investigate the asymptotics of multifractals, and discover a new way to use fractal analysis to characterize geometry.

The standard technique used to determine whether an image is fractal is to cover it with a grid of square boxes of size L and count the number of occupied boxes, N. For a fractal, $N \propto L^D$ where D is the fractal dimension and is non-integer. The box-counting curve (a plot of $\log N$ against $\log L$) is therefore a straight line with slope D. According to Taylor *et al.* [6] the box-counting curves of Pollock paintings meet the following criteria: (1) there are two fractal dimensions, $D_D < D_L$, where D_D is the fractal dimension for boxes smaller than a transition length L_T, and D_L for boxes larger than L_T; (2) $L_T > 1.0$ cm; (3) the fits to the box-counting data are low noise with $\chi < 0.026$; (4) for multi-colored paintings each colored layer as well as the composite painting all satisfy criteria (1-3). Fractal authentication is based on the claim that all Pollock drip paintings satisfy these criteria. In addition it is also claimed that these characterisics are exclusive to Pollock, arising from his unique mastery of chaotic motion [2, 3, 4, 5, 6].

In previous work [7] we identified several problems with the fractal analysis of Taylor *et al.*: (i) an insufficient range of box sizes was used to establish fractal behaviour; (ii) it is mathematically impossible for the visible portion of each layer and the composite to separately behave as fractals in a multilayered painting; (iii) χ depends on the magnification factor used in box-counting and is therefore not intrinsic to the image.

In this Letter, we first focus on whether, regardless of these issues, the box-counting curve can be used for authentication.

We begin our discussion of image analysis with the problem of color separation. A digital image in RGB mode describes each pixel by three numbers, its R (red), G (green), and B (blue) values, which lie in the range 0 to 255. Naively one might expect individual colors to occupy distinct regions of RGB space, and to separate a particular color from the rest, one can simply define a median RGB value and collect the pixels that lie within a certain radius. This is precisely the color separation procedure used by Mureika *et al.* [8]. It is easy to implement but does not work particularly well [16], as illustrated in Fig 1.

As color separation is a delicate task, we developed two independent techniques we call the Photoshop method and the Adaptive RGB Mesh method, which are both described in detail in the accompanying EPAPS Document [9]. Results from the two methods are in excellent agreement [9].

We now embark on a discussion of specific paintings, starting with three famous works by Pollock. A gallery of all paintings discussed below and their box-counting data can be found in the accompanying
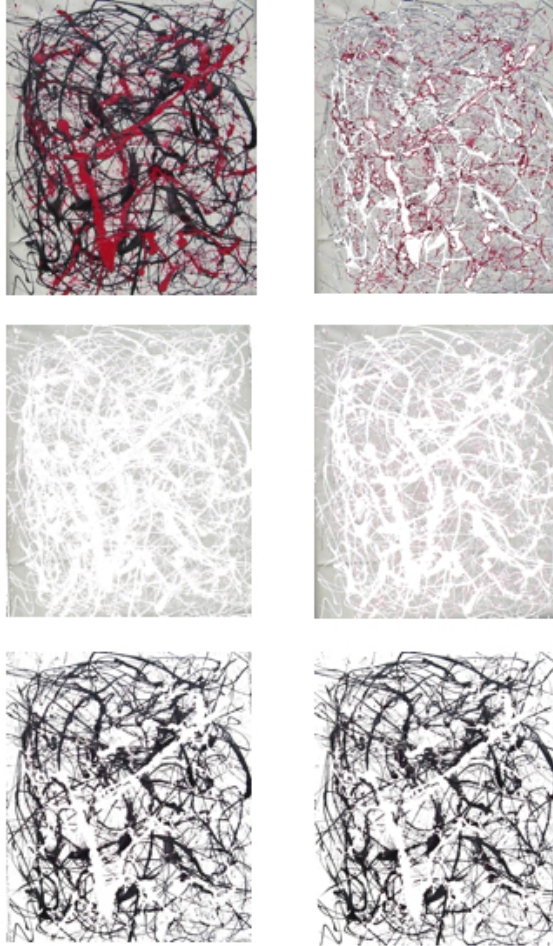
Figure 1: **Color Separation** *Composition with Red and Black* (top left) and its background layer as obtained with the color separation method of Mureika *et al.* [8] (top right). The background layer for the same painting as obtained by Photoshop (middle left) and RGB Mesh (middle right) methods. The black layer as obtained by Photoshop (bottom left) and RGB Mesh (bottom right) methods.
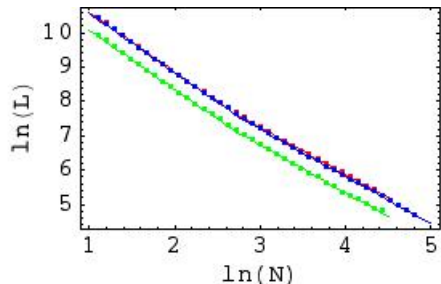
Figure 2: ***Untitled* (ca 1950)** (a) Untitled (ca 1950) by Jackson Pollock, Enamel on paper, 28.3 × cm 150.3 cm, Staatsgalerie Stuttgart [10]. The digital image has 1145 × 5150 pixels. [**Image will be inserted following publication**]. (b) Box-counting curves for *Untitled* with color separation by the Photoshop method (red) and adaptive RGB mesh (blue) and cropped image (green). Because of the awkward aspect ratio of this painting we were forced to scan it as two sub-images which we then merged. The cropped image here corresponds to the larger of the two sub-images.

EPAPS document [9].

We chose to analyze *Free Form* (1946) because it had previously been included by Taylor *et al.* [6] in the list of canonical Pollock paintings from which the fractal authentication criteria were developed [17]. Surprisingly, we find that *Free Form* does not conform perfectly to the fractal authentication criteria; specifically we find that for the composite image $L_T <1.0$ cm [9]. Although *Free Form* does not pass a rigorous application of the fractal authentication criteria, ref [6] describes a more relaxed procedure called force-fitting. Force fitting imposes the constraint that $L_T > 1.0$ cm, thereby automatically satisfying authentication criterion (2). Thus authentication is reduced to checking that the other criteria are fulfilled. We find that force fitting *Free Form* does not significantly change D_D, D_L, or χ and these parameters do remain consistent with fractal authentication criteria. Thus adopting the more relaxed fractal authentication criterion, based solely on fractal analysis one would conclude that *Free Form* is indeed authentic.

No such stratagem avails for *Untitled* (ca 1950), shown in Fig 2, which fails the fractal authentication test in a more spectacular way. Force-fitting offers recourse for a painting with $L_T < 1.0$ cm, and can be decreased by trimming the range of box sizes; thus anomalous dimensions $D_D > D_L$ is the clearest sign that a painting fails the fractal authenication test. It is in this respect that Pollock's *Untitled* (ca 1950) fails. *The Wooden Horse: Number 10A, 1948* (1948) is another Pollock painting that unambiguously fails to satisfy the fractal authentication test. It has anomalous dimensions in two of six color layers. Thus, based solely on fractal analysis, one would conclude neither of these paintings (both of which are undisputed Pollock paintings) are authentic Pollocks.

Interestingly, two of the 25 extant paintings in the cache discovered by Alex Matter resemble *Free Form* and *Wooden Horse*. Taylor *et al.* analyzed six paintings from the Matter cache and found that none conformed to fractal authentication criteria [1]. We find that the fractal characteristics of the Matter paintings which resemble *Free Form* and *Wooden Horse* bear a striking similarity to the fractal characteristics of the two analogous Pollock paintings: the painting that resembles *Free Form* meets all the fractal authentication criteria provided we force-fit the composite layer, and the painting that resembles *Wooden Horse* fails unambiguously by having anomalous dimensions in two out of six layers.

In [7] we demonstrated that crude drawings such as *Untitled 5* would be mistaken for authentic Pollocks by a computer using fractal analysis for authentication. Although *Untitled 5* seriously undermined fractal authentication, it remained to show that actual drip paintings that are unquestionably not by Pollock too can satisfy the fractal authentication criteria; it is this step of the argument we now present. The artists we commissioned, Alexandra Ash and Michael Hallen, studied Pollock's technique and rendered nine drip paintings. Of these we have so far analysed two paintings, chosen for the relative ease with which they could be color separated. As the numbers show [9], both paintings satisfy all fractal authentication criteria comfortably, even without the force-fitting required for *Free Form*.

We now turn to two problems in fractal mathematics motivated by our analysis of drip paintings but with results of broader significance. Whether fractal analysis allows authentication of drip paintings has
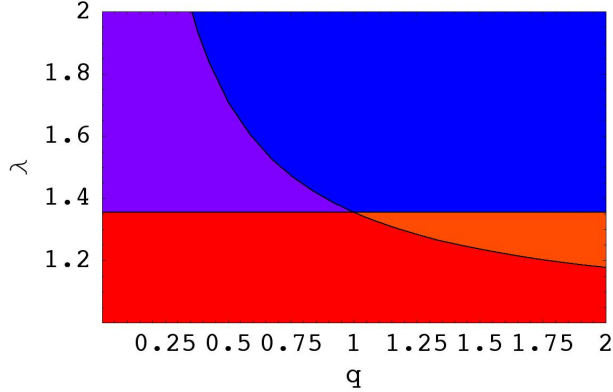
3

Figure 3: **Phase Diagram for overlapping Cantor Dusts** A 1/3 Cantor dust is iterated $2\Lambda_2$ times and a 3/9 Cantor dust is iterated Λ_1 times. The geometry of their union is characterised by a single parameter $\lambda = \frac{\Lambda_2}{\Lambda_1}$. The behaviour of the multifractal spectrum of dimensions D_q of the union is encapsulated by the phase diagram depicted here. In the red phase the 1/3 dust completely dominates and $D_q = D_{1/3} = 0.6309$ Similarly in the blue phase the 3/9 dust dominates and $D_q = D_{3/9} = 0.5$. But in the purple region the 3/9 dust dominates on long length scales and the 1/3 on short scales; the effective dimension D_q crosses over from $D_{3/9}$ to $D_{1/3}$. In the orange region the crossover is from 3/9 to 1/3. If we focus on the shortest scales for a fixed $\lambda < \lambda_c = 1.354\ldots$, D_q jumps from $D_{1/3}$ to $D_{3/9}$ as q is increased. Similarly for fixed $\lambda > \lambda_c$, the jump is from $D_{3/9}$ to $D_{1/3}$. Thus on the shortest scales the union of two fractals is revealed to be a complex multifractal. The vertical line $q = 0$ corresponds to the ordinary fractal dimension. Along this line we find relatively trivial behaviour: the 1/3 dust always dominates and the union behaves asymptotically as a fractal with dimension $D_{1/3}$.

immediate and significant financial implications in the art world, but the mathematical results presented here have more enduring scientific importance.

First consider asymptotic scaling behaviour of composites of ideal fractals, e.g., the union of a middle 1/3 Cantor dust (dimension $D_{1/3} = 0.6309\ldots$) and the 3/9 dust (dimension $D_{3/9} = 0.5$) (see ref [7] and [9]). The 1/3 dust is iterated $2\Lambda_2$ times; the 3/9 dust, Λ_1 times. The geometry of the union is controlled by $\lambda = \frac{\Lambda_2}{\Lambda_1}$ .These dusts are ideal fractals since the range over which fractal behavior is seen can be made arbitrarily large. In previous work [7] we showed that the union is not fractal because its box counting curve is not a simple power law except in the asymptotic limit of very small box sizes. In that limit, the number of boxes filled with 1/3 dust overwhelms the number filled with 3/9 dust because $D_{1/3} > D_{3/9}$. Thus the union behaves as a fractal with dimension $D_{1/3}$.

The full asymptotic complexity of the union is brought out by consideration of the spectrum of multifractal dimensions, D_q. On small scales the 1/3 dust determines the fractal dimension, D_0, but the 3/9 dust can control D_q for sufficiently large q. Fig 3 shows that, except in the trivial instances that one dust overwhelms the other, the union is not scale invariant over the same range as the constituent fractals. Moreover for fixed λ, varying q can produce a discontinuous jump in the dimension D_q. By contrast, for an ideal fractal D_q is independent of q. For generic multifractals D_q varies smoothly with q. Discontinuities in D_q are of great interest due to the thermodynamic analogy between multifractal dimensions and phase transitions[11]. Thus the union is revealed to be a complex multifractal on the shortest length scales; details of the derivation of the results quoted here are relegated to [9].

Let us briefly consider the relevance of this analysis to paintings.Taylor *et al.* [6] assert that the composite of two colored layers is a fractal with a dimension that is different from either of its constituent layers. This assertion is mathematically impossible. It is presumably an artefact of fitting power law behaviour to data over a limited range.

The box-counting curve is a staircase function, because the number of filled boxes is an integer that increases monotonically as the box size is reduced. Staircase functions abound in mathematics and physics, e.g., $\Pi(x)$, the number of primes less than x [12]; $N(E)$, quantum energy levels less than E [13]; and $n(s)$, zeta function zeros whose imaginary part lies between zero and s [13]. In all these cases there has been a

concerted effort to determine a smooth fit through the staircase as well as to characterise the deviations of the staircase from this smooth fit. For example Gauss found a smooth asymptotic fit to $\Pi(x)$. The smooth form of $N(E)$ is basic to statistical mechanics. The deviations from regularity of $N(E)$ show remarkable universal behaviour encapsulated by random matrix theory. The deviation statistics of $n(s)$ are the subject of a conjecture, ancillary to the Riemann hypothesis, due to Dyson and Montgomery. By contrast, hitherto in fractal analysis the focus has been on finding a smooth power law fit to the staircase and extracting the exponent (the fractal dimension); we now study the deviations from regularity.

For simplicity, instead of the box-counting dimension we analyse a closely related variant [14], the covering dimension. Here the staircase $N(\varepsilon)$ is the number of intervals of size ε needed to cover the fractal. We first study a unit line segment for which $N(\varepsilon) \approx 1/\varepsilon$, corresponding to a covering dimension of 1. Consider the sequence of interval sizes $\varepsilon_n \equiv \varepsilon_0/C^n$ where $n = 1, \ldots, M$. Here ε_0 is the largest interval size and C is the reduction factor. We define $\chi_n \equiv N(\varepsilon_n) - 1/\varepsilon_n$, the deviation of the exact counting staircase from the smooth fit. It is easy to show that as $M \to \infty$, χ^2 (the mean value of χ_n^2) vanishes [9]. Thus the counting curves of line segments are essentially noiseless. Similar analysis for the middle third Cantor dust shows that the deviates are uniformly distributed over a finite interval and have a non-zero mean square value [9]. Thus the fractal counting curve of the $1/3$ dust is intrinsically noisy. Intuitively we can understand that Euclidean objects would be noiseless because the deviations from regular behaviour originate at boundary points. A Euclidean segment has only two boundary points; fractals have an infinity. We conjecture that counting curves are generically noiseless for Euclidean objects whereas they have well defined deviate statistics and mean squared deviation for fractals. Like simple random number sequences [15], the successive deviates for the $1/3$ dust are given by a formula that involves modular arithmetic. The $1/3$ dust deviates are highly correlated but it is tantalising to speculate that there might be other fractals whose counting curves could serve as pseudo-random number sources.

Again we briefly consider the implications of these findings for paintings. For fractals χ^2 is pseudo-random and for generic images it may be C dependent; hence the use of χ^2 as a characteristic of paintings advocated in ref [6] is inappropriate. Taylor *et al.* suggest that Pollock's works are high quality fractals because they have small χ^2 values [6]. Our analysis shows that it is in fact Euclidean objects that have low χ^2.

In summary, while in [7] we briefly described various shortcomings of fractal analysis as an authentication tool, and identified a number of mathematical inconsistencies lurking in the mere application of fractal analysis to multi-colored drip paintings, we have shown here that (i) amateur artists seeking to emulate Pollock's technique can successfully create paintings which possess the fractal signature said to be unique to Pollock; and (ii) even authentic Pollock paintings fail to possess his fractal signature. Contrary to Taylor *et al.*, we also find at least one Matter painting possesses Pollocks fractal signature. Finally, our analysis has initiated a study of the statistics of counting staircases, a new topic in fractal mathematics that invites much further exploration.

References

[1] A. Abbott "Fractals and art: In the hands of a master", Nature **439**, 648 (2006).

[2] Taylor, R.P., Micolich, A.P., and Jonas, D. "Fractal Analysis of Pollock Drip Paintings", Nature **399**, 422 (1999).

[3] Taylor, R.P., Micolich, A.P., and Jonas, D., "Fractal Expressionism: Art, Science and Chaos", Physics World **12**, 15 (1999).

[4] Taylor, R.P., Micolich, A.P., and Jonas, D., "The Construction of Pollock's Fractal Drip Paintings", Leonardo **35**, 203 (2002).

[5] Taylor, R.P., "Fractal ExpressionismWhere Art Meets Science", pp. 117, in: Casti, J., and Karlqvist, A. (Eds.), Art and Complexity (Elsevier Press, Amsterdam, 2003).

[6] R.P. Taylor *et al.*, "Authenticating Pollock Paintings Using Fractal Geometry", Pattern Recognition Letters **28**, 695 (2007).

[7] K. Jones-Smith and H. Mathur, "Revisiting Pollock's drip paintings", Nature **444**, doi:10.1038/nature05398 (2006).

[8] J.R. Mureika, C.G. Dyer and G.C. Cupchik, Phys Rev **E72**, 046101 (2005).

[9] See attached EPAPS Document for a description of methods, a gallery of the paintings analysed here, and complete boxcounting data for all the analysed paintings.

[10] D. Anfam, S. Davidson and M.Ellis, *No Limits, Just Edges: Jackson Pollock Paintings on Paper* (Guggenheim Museum 2005).

[11] E. Ott, *Chaos in Dynamical Systems* (Cambridge University Press, Cambridge, 2002).

[12] G. H. Hardy and E.M. Wright, *An Introduction to the Theory of Numbers* (Oxford University Press, Oxford, 1979).

[13] M.L. Mehta, *Random Matrices* (Academic Press, San Diego, 1991).

[14] M.F. Barnsley, *Fractals Everywhere* (2nd edition) (Academic Press Professional, Boston, 1993).

[15] W.H. Press, S.A. Teukolsky, W.T. Vetterling and B.P. Flannery, *Numerical Recipes* (2nd edition) (Cambridge University Press, Cambridge, 1992).

[16] Unfortunately Taylor *et al.* [2, 3, 4, 5, 6] have nowhere provided sufficient information about their color separation method to allow us to caliberate our techniques against theirs.

[17] It appears on the list of 17 paintings that were the basis of the criteria in a preprint version of ref [6] but not in the published version.

EPAPS AUXILIARY MATERIAL: METHODS

COLOUR SEPARATION

In a digital image the colour of each pixel is described by three numbers each of which lies in the range 0 to 255: its R, G, B values. Thus colour or RGB space may be viewed as a cube. Each pixel corresponds to a point inside this cube. Naively one might expect that pixels of the same colour would clump together in colour space and pixels of different colours would be well-separated. But in fact human colour perception is highly non-linear: in some regions of colour space a small variation in the RGB values can lead to a dramatic change in perceived colour; in other regions, large variations in the RGB values correspond to essentially no change in the perceived colour. Thus different colours form large almost interpenetrating regions in colour space (see fig 4) and colour separation is therefore a formidable task.

Consider separating a painting such as *Composition with Red and Black* into its red and black layers. As discussed above the red pixels and black pixels form irregular, interpenetrating swarms in RGB colour-space. The simplest approach to colour separation is to place two non-intersecting spheres inside colour space and to count the pixels inside one as red and the ones inside the other as black. The location of the spheres and their size are fitting parameters that can be adjusted to ensure that each sphere encloses as many of the right kind of pixels as possible and as few of the wrong sort. Typically, though either different colours get mixed, or parts of a layer get left behind as background residue, as illustrated in figure 1 of the paper. Thus this method which was used in ref [8], has few virtues besides ease of implementation. (Parenthetically we note that fig 1 in the paper was generated by taking the center of the black sphere at (R, G, B) = $(41, 40, 41)$ and the red sphere at $(161, 15, 34)$. The radius of both spheres was taken to be 40. The centers were chosen by using the median (R,G,B) values, as computed using Photoshop, and the radius was optimised by trial and error).

In the Photoshop method the user selects a pixel using a tool called magic wand. All pixels within a narrow user-controlled RGB range (the "tolerance") of the selected pixel are then highlighted by magic wand. If they are all from the desired layer they are transferred to a blank background. The user continues to select
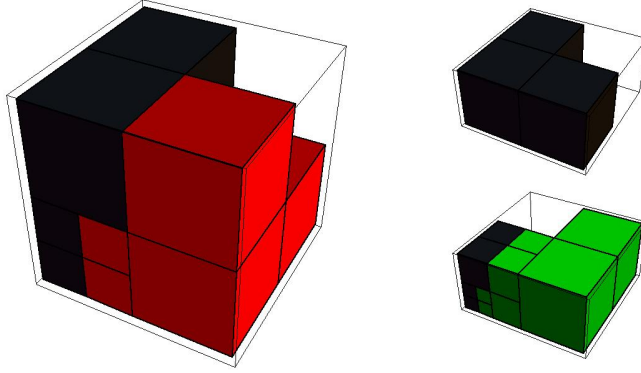
Figure 4: The partition of the the RGB cube into red and black regions for *Composition with Red and Black* (left). The blank portion of the RGB cube is occupied by pixels from the essentially white background. The partition of the RGB cube into regions occupied by black and background pixels for the Matter painting that resembles *Free Form* is shown to the right. The region of the RGB cube occupied by background pixels is shown in green; by the white layer, left blank. The RGB cube has been sliced to reveal a cutaway. Note how the different coloured layers occupy complex interpenetrating regions of RGB colour space.

pixels in this way until the entire layer has been transferred. By judicious selection of pixels and use of a narrow tolerance accidental selection of pixels from a different layer can be minimised. Schematically the contrast between the simple method of the previous paragraph and the Photoshop method is that the former attempts to enclose the swarm of red pixels within a single well-chosen sphere; the Photoshop method covers it with a series of small spheres and can therefore accomodate the large extent and the irregular shape.

In the adaptive RGB mesh approach the colour cube is divided up into eight smaller cubes which are designated with a binary address. 011 for example refers to the sub-cube where $0 < R < 127, 128 < G < 255$ and $128 < B < 255$; 101, where $128 < R < 255, 0 < G < 127$ and $128 < B < 255$; and so forth. The user then examines an image in which only pixels from a single subcube are displayed with their true colours; the other pixels are displayed as white or another user selected uniform background colour. If this image is seen to contain pixels from a single layer the user records that the entire subcube contains only pixels of one colour. For example, for *Composition with Red and Black* it was found that 001, 010 and 011 contained only black pixels; 100, 101 and 110 contained only red; 111 contained only background. But if a subcube contains more than one colour, as does 000, it is further subdivided into eight cubes, and the process is reiterated as many times as needed. *Composition in Red and Black* for example required three levels of subdivision. The binary address notation for higher level subdivisions works in the same way. For example the level two sub-cube with binary address 01-10-11 refers to the region where $64 < R < 127, 128 < G < 191$ and $192 < B < 255$.

The two methods have complementary strengths. The Photoshop method, if skillfully deployed, is faster. Also it allows the user to make better use of spatial information when deciding which pixels to include in a given layer. The adaptive RGB mesh on the other allows for systematic refinement and provides a detailed characterisation of the way in which colour space is partitioned into the layers of the drip painting. The code we developed to implement RGB mesh included a number of features including the ability to count the pixels in each sub-cube to determine their relative importance and the ability to regroup and consolidate pixels spatially for easier viewing. In principle the program could be refined to make fuller use of spatial information but in practice we found that results adequate for our needs could be obtained without this feature.

CONSTRUCTION OF CANTOR DUSTS

The 1/3 dust [11, 14] is constructed by starting with a unit line segment and removing the middle third. At the second iteration the middle third of the two surviving segments is removed; at the third iteration, the middle third of the four surviving segments. After Λ iterations the set consists of 2^Λ segments each of

length $1/3^\Lambda$. This set behaves as a fractal on length scales between 1 and $1/3^\Lambda$. By increasing Λ we can make this range arbitrarily large, thus approaching a mathematical fractal.

There is a useful way to label segments using base 3 numbers. At the first iteration we label the left, middle and right thirds of the initial unit segment as 0, 1 and 2 respectively. We then label the left, middle and right thirds of the left third 00, 01, and 02. Proceeding in this way we see that after the second iteration the four segments that survive have the labels 00, 02, 20 and 22. After Λ iterations there are 3^Λ segments. The address of each segment is a base 3 number of Λ digits. The segments that survive are the ones that have only 0s and 2s in their base three addresses.

The 3/9 dust is constructed by starting with a unit line segment, dividing it into nine equal segments, and retaining only the first, fifth and ninth segments [7]. At the second iteration the surviving segments are divided up into ninths and in each case only the first, fifth and ninth subsegments are retained. After Λ iterations the set consists of 3^Λ segments each of length $1/9^\Lambda$. Segments in the 3/9 dust can be labelled by using base 9 numbers. For example, after the first iteration the segments that are retained are labelled 0, 4 and 8. After Λ iterations the segments will have labels that consist of base 9 numbers of Λ digits. The segments that belong to the 3/9 dust will have only 0s, 4s and 8s in their address.

Another point of view on the 1/3 dust is that it is obtained by taking the unit segment, dividing it up into ninths, and retaining the first, third, seventh and ninth segments. From this point of view, after 2Λ iterations the dust consists of 4^Λ segments each of length $1/9^\Lambda$. From this perspective segments can be labelled by base 9 numbers. For example, after the first iteration the four surviving segments are 0, 2, 6 and 8. After 2Λ iterations the segments will have labels that consist of base nine numbers of Λ digits. The ones that belong to the 1/3 dust will have only 0s, 2s, 6s and 8s in their address. This viewpoint on the 1/3 dust is useful when studying its union and intersection with the 3/9 dust.

ASYMPTOTIC ANALYSIS OF OVERLAPPING FRACTALS

(a) Two Cantor Dusts: First we summarize our results, then we outline their derivation. Consider the union of a 1/3 Cantor dust iterated $2\Lambda_2$ times and a 3/9 dust iterated Λ_1 times with $\lambda \equiv \Lambda_2/\Lambda_1 \geq 1$. This construction results in 4^{Λ_2} segments each of length $1/9^{\Lambda_2}$ and $3^{\Lambda_1} - 2^{\Lambda_1}$ segments each of length $1/9^{\Lambda_1}$. The total length of the resulting object is therefore

$$l_{\text{tot}} = 4^{\Lambda_2}\frac{1}{9^{\Lambda_2}} + (3^{\Lambda_1} - 2^{\Lambda_1})\frac{1}{9^{\Lambda_1}}. \tag{1}$$

We suppose that the resulting object has unit mass and that the density (mass per unit length) is uniform and hence equal to $1/l_{\text{tot}}$.

We now cover this object with boxes of size $\epsilon = 1/9^\mu$ where $1 \leq \mu \leq \Lambda_1$. It turns out that there are three classes of filled boxes. The number of boxes of each class and the mass contained within each box are given by

$$
\begin{aligned}
n_A &= 2^\mu, \\
m_A &= \left[4^{\Lambda_2-\mu}/9^{\Lambda_2} + (3^{\Lambda_1-\mu} - 2^{\Lambda_1-\mu})/9^{\Lambda_1}\right]/l_{\text{tot}}; \\
n_B &= 4^\mu - 2^\mu, \\
m_B &= \left[4^{\Lambda_2-\mu}/9^{\Lambda_2}\right]/l_{\text{tot}}; \\
n_C &= 3^\mu - 2^\mu, \\
m_C &= \left[3^{\Lambda_1-\mu}/9^{\Lambda_1}\right]/l_{\text{tot}}.
\end{aligned}
\tag{2}
$$

Instead of the number of filled boxes of size ϵ, in multifractal analysis[13] we consider the generalised box count $N(q, \epsilon)$ defined as

$$\ln N(q, \epsilon) = \frac{1}{1-q}\ln\sum_i m_i^q. \tag{3}$$

Here q is a continuous real parameter, m_i is the mass in the ith occupied box, and the sum is over all filled boxes. For multifractals it is expected that $N(q, \epsilon)$ will vary as a power of box size ϵ. Thus we may extract

the multifractal spectrum of dimensions by computing

$$D_q = \lim_{\epsilon \to 0} \frac{\ln N(q, \epsilon)}{\ln(1/\epsilon)}. \tag{4}$$

Evidently $N(q, \epsilon)$ is equal to the number of filled boxes for $q = 0$ and D_0 is just the ordinary fractal dimension. Making use of eq (2), it follows that for the overlapping Cantor dusts

$$N(q, \epsilon) = \frac{1}{1-q} \ln(n_A m_A^q + n_B m_B^q + n_C m_C^q). \tag{5}$$

Eq (5) is the central result of this section. It allows us to plot the generalised box counting curve of the union of the Cantor dusts as well as to determine the asymptotic behaviour.

The phase diagram for the overlapping Cantor dusts can be constructed by straightforward asymptotic analysis of eq (5). It is easy to argue that class B and class C boxes generally dominate the contribution of class A to the generalised box count. When class B dominates class C the generalised box count approaches that of a pure 1/3 dust; when class C dominates class B, that of a pure 3/9 dust. First consider the case $0 < q < 1$. In this case for $1 < \lambda < \lambda_c$ the 1/3 dust dominates; for $\lambda > \lambda^+$ the 3/9 dust dominates. For $\lambda_c < \lambda < \lambda^+$ there is a crossover: the 3/9 dust dominates for $\mu < \mu_c$ and the 1/3 dust dominates for $\mu > \mu_c$. Here $\lambda_1 = \ln 3 / \ln(9/4) = 1.354\ldots$, λ^+ is the curve defined by $\lambda^+ = 1 + (\lambda_c - 1)/q$, and μ_c is given by

$$\mu_c = \Lambda_1 \frac{q}{1-q} \frac{[\lambda \ln(9/4) - \ln 3]}{\ln(4/3)}. \tag{6}$$

Note that μ_c/Λ_1 varies from zero to one as λ varies from λ_c to λ^+.

Similarly for $q > 1$ we find that for $\lambda > \lambda_c$ the 3/9 dust dominates. For $\lambda^+ > \lambda > 1$ the 1/3 dust dominates. For $\lambda^+ > \lambda > \lambda_c$ there is a crossover: the 1/3 dust dominates for $\mu < \mu_c$ and the 3/9 for $\mu > \mu_c$ where μ_c is given by eq (6).

Now we outline the derivation of these results. For simplicity we only consider the union of two Cantor dusts with $\Lambda_2 = \Lambda_1 = \Lambda$; the generalisation is straightforward. We adopt the notation that $n = 0$ or 8, $m = 2$ or 6, $\nu = 0, 4$, or 8 and $N = 0, 2, 6$ or 8. After the first iteration of the 3/9 dust and the second iteration of the 1/3 dust the base nine addresses of the surviving segments are 0, 2, 4, 6 and 8. In terms of the notation above the addresses are n_1, m_1 or 4. At the next iteration the possible addresses are: $n_1 n_2$; $n_1 m_2$, $m_1 N_2$; n_1 4 or 4 ν_2. By working out a few iterations with this notation it is easy to deduce that once an m appears in an address the subsequent integers in the address must be N's. Once a 4 appears, the subsequent integers are ν's. On the other hand, an n can be followed by n, m or 4. Thus after Λ iterations the segments fall into three classes with binary addresses that (A) are composed entirely of n's, (B) include at least one m and (C) include at least one 4. By induction we can show that $n_A = 2^\Lambda$, $n_B = 4^\Lambda - 2^\Lambda$ and $n_C = 3^\Lambda - 2^\Lambda$. Since all segments are of length $1/9^\Lambda$ we can easily write down an expression for the total length of the object l_{tot} which is in agreement with eq (1)

Now suppose we cover the object with boxes of size $1/9^\mu$ where $\mu < \Lambda$. The boxes themselves fall into the three classes A, B, and C depending on their base nine addresses. A class A box has only n's in its base nine address. A segment that lies in a class A box has the same sequence of n's for the first μ digits of its base nine address. The remaining $\Lambda - \mu$ digits may be n's, m's or 4s. Thus the segments contained in a class A box effectively constitute the union of a 1/3 and 3/9 dust that is iterated $\Lambda - \mu$ times. Therefore it contains $4^{\Lambda-\mu} + 3^{\Lambda-\mu} - 2^{\Lambda-\mu}$ segments. Moreover, since the address of a class A box is a string of n's of length μ, evidently there are 2^μ class A boxes. In the same way we can show that there are $4^\mu - 2^\mu$ boxes of class B and $3^\mu - 2^\mu$ boxes of class C. The segments in a class B box have a base nine address that coincides with that of the box for the first μ places. According to the rules above this is followed by a string of N's of length $\Lambda - \mu$. Thus a class B box contains $4^{\Lambda-\mu}$ segments. Similarly a segment in a class C box has a base nine binary address that coincides with that of the box for the first μ places. Thereafter it is a string of ν's of length $\Lambda - \mu$. Thus a class C box contains $3^{\Lambda-\mu}$ segments. With this we have derived all the information in eq (2) for the special case $\Lambda_1 = \Lambda_2 = \Lambda$. The derivation is readily generalised to the case $\Lambda_1 \neq \Lambda_2$.

Note also that for this special case we have also shown that the number of filled boxes of size $1/9^\mu$ is $4^\mu + 3^\mu - 2^\mu$. This is the result plotted in fig 1 of ref [7] to illustrate that the box counting curve for the union of two fractals is not a simple power law.

(b) Euclidean Island in sea of Cantor Dust: We now briefly outline a second soluble example of the union of two objects with distinct fractal dimensions. The set we consider consists of a $1/3$ dust that is initially iterated Λ_1 times. The segment to the extreme right (the Euclidean island) is now left fixed. The other surviving segments are further subdivided a further Λ_2 times to form a fine $1/3$ dust. The Euclidean island has a length $1/3^{\Lambda_1}$. The dust consists of $2^{\Lambda_1 + \Lambda_2} - 2^{\Lambda_2}$ segments each of length $1/(3^{\Lambda_1 + \Lambda_2})$. The total length of the object is therefore

$$l_{\text{tot}} = \frac{1}{3^{\Lambda_1}} + (2^{\Lambda_1 + \Lambda_2} - 2^{\Lambda_2}) \frac{1}{3^{\Lambda_1 + \Lambda_2}}. \tag{7}$$

Let us now cover the object with boxes of size $\epsilon = 1/(3^{\Lambda_1 + \mu})$ where $0 \leq \mu \leq \Lambda_2$. The occupied boxes fall into class (A) that cover dust and class (B) that cover the Euclidean island. It is easy to see that

$$n_A = 2^{\Lambda_1 + \mu} - 2^{\mu}, \qquad m_A = \frac{1}{l_{\text{tot}}} 2^{\Lambda_2 - \mu} \frac{1}{3^{\Lambda_1 + \Lambda_2}};$$

$$n_B = 3^{\mu}, \qquad m_B = \frac{1}{l_{\text{tot}}} \frac{1}{3^{\Lambda_1 + \mu}}. \tag{8}$$

Thus the generalised box count defined in eq (3) is given by

$$\ln N(q, \epsilon) = \frac{1}{1 - q} \ln(n_A m_A^q + n_B m_B^q). \tag{9}$$

Eq (9) is the main result of this subsection. It allows us to plot the generalised box counting curve for this composite object as well as to analyse its asymptotic behaviour.

The phase diagram implied by eqs (8) and (9) can be obtained by straightforward asymptotic analysis. The geometry of the union of the island and dust is controlled by a single parameter $\lambda \equiv \Lambda_1 / \Lambda_2$. First consider $0 \leq q < 1$. It is convenient to define $\lambda_0 = \ln(3/2)/\ln 2 = 0.58496\ldots$. Now for $\lambda < q\lambda_0$ the island dominates and the dimensions $D_q = 1$. For $\lambda > \lambda_0$ the dust dominates and the dimensions $D_q = D_{1/3}$, the fractal dimension of the $1/3$ dust. For $q\lambda_0 < \lambda < \lambda_0$ the dust dominates for $\mu < \mu_0$, the island for $\mu > \mu_0$; the slope of the generalised boxcounting curve crosses over from $D_{1/3}$ to 1. Here the crossover scale μ_0 is given by

$$\mu_0 = \Lambda_2 \frac{1}{1 - q} \frac{\lambda - q\lambda_0}{\lambda_0} \tag{10}$$

Now consider $q > 1$. In this case for $\lambda < \lambda_0$ the island dominates and the dimensions $D_q = 1$. For $\lambda > q\lambda_0$ the dust dominates and $D_q = D_{1/3}$. For $\lambda_0 < \lambda < q\lambda_0$ the island dominates for $\mu < \mu_0$ and the dust for $\mu > \mu_0$; the slope of the generalised box-counting curve crosses over from 1 to $D_{1/3}$. This information is encapsulated in the phase diagram shown in fig 5.

COUNTING STATISTICS

(a) Line segment: $N(\epsilon)$ is the smallest number of segments required to cover a unit line segment [14]. Evidently

$$N(\epsilon) = \text{Ce}\left(\frac{1}{\epsilon}\right) \tag{11}$$

where $\text{Ce}(x)$ is the smallest integer that is greater than or equal to x. In other words Ce rounds up its argument. $N_{\text{smooth}}(\epsilon) = 1/\epsilon$ is a smooth fit through this counting staircase. From the definition

$$\chi(\epsilon) = \ln N(\epsilon) - \ln N_{\text{smooth}}(\epsilon) \tag{12}$$

and eq (11) it is easy to see that for small ϵ

$$\chi(\epsilon) = \epsilon \Delta(\epsilon). \tag{13}$$

Here $\Delta(\epsilon) = \text{Ce}(1/\epsilon) - 1/\epsilon$ lies between zero and one since it represents the amount of round up.
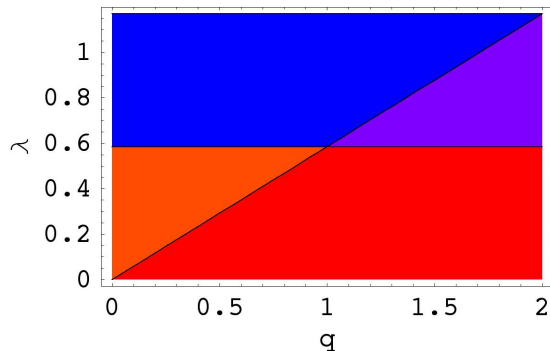
Figure 5: **Phase Diagram for Euclidean segment and Cantor Dust:** The geometry of the union of the two sets is controlled by a single parameter $\lambda = \Lambda_1/\Lambda_2$ where Λ_1 is the scale of the island and $\Lambda_1 + \Lambda_2$ of the dust as explained in the text. The diagram shows the behaviour of the multifractal spectrum of dimensions D_q as a function of λ and q. In the red phase the island dominates completely and $D_q = 1$. Similarly in the blue phase the 1/3 dust dominates and $D_q = D_{1/3}$. But in the purple region the island dominates on long scales while the dust dominates on short scales; the effective dimension D_q crosses over from 1 to $D_{1/3}$. In the orange region the dust dominates on long length scales and the island on short scales; the effective dimension D_q crosses over from $D_{1/3}$ to 1. If we fix λ, D_q jumps discontinuously as a function of q over an appropriate range of length scales. Thus the union of the two sets is a complex multifractal on these scales.

We now sample the counting curve at a sequence of interval sizes $\epsilon_n = \epsilon_0/C^n$ where $C > 1$ is a reduction factor, ϵ_0 is the largest interval size considered and $n = 0, 1, 2, \ldots, M-1$. The quantities of interest are $\chi_n = \chi(\epsilon_n)$, the deviations of the counting curve from the smooth fit at the sampled interval sizes. As usual the mean square deviation is given by

$$\chi^2 = \frac{1}{M} \sum_{n=0}^{M-1} \chi_n^2. \tag{14}$$

It is easy to derive the bound

$$\chi^2 \leq \frac{\epsilon_0^2}{M} \frac{1}{1 - 1/C^2} \tag{15}$$

revealing that $\chi^2 \to 0$ as $M \to \infty$. Thus Euclidean staircases are essentially noiseless.

(b) Cantor dust: The analysis of the middle third Cantor dust proceeds exactly in parallel to the Euclidean line segment. The exact staircase function is given by

$$
\begin{aligned}
N(\epsilon) &= 2^{n(\epsilon)} \\
\text{where } n(\epsilon) &= \mathrm{Ce}\left[\frac{\ln(1/\epsilon)}{\ln 3}\right].
\end{aligned}
\tag{16}
$$

$N_{\text{smooth}} = 1/\epsilon^{D_{1/3}}$ is a smooth fit through this staircase where $D_{1/3} = \ln 2/\ln 3$ is the fractal dimension of the middle third dust. From the definition of $\chi(\epsilon)$, eq (12), and the exact staircase, eq (16), it follows that

$$\chi(\epsilon) = \ln 2 \left(\mathrm{Ce}\left[\frac{\ln(1/\epsilon)}{\ln 3}\right] - \frac{\ln(1/\epsilon)}{\ln 3} \right). \tag{17}$$

By sampling the counting curve in the usual way we obtain the sequence of deviates

$$\chi_n = \ln 2 \left(\mathrm{Ce}\left[\frac{n \ln C}{\ln 3} - \frac{\ln \epsilon_0}{\ln 3}\right] - \left[\frac{n \ln C}{\ln 3} - \frac{\ln \epsilon_0}{\ln 3}\right] \right). \tag{18}$$

This leads us to contemplate expressions of the form

$$\xi_n = \mathrm{Ce}(an + b) - (an + b). \tag{19}$$

11

Let us make the rational choice $a = p/q$ where, without further loss of generality, we may take p and q to be coprime and $p < q$. From eq (19) it is easy to see that ξ_n are a uniformly spaced sequence of q points on the unit interval. Thus the χ_n's are seen to be uniformly distributed and highly correlated.

With suitable rescaling eq (19) may be written in the form $I_{n+1} = (\alpha n + \gamma) \pmod{m}$ where $I_n = q\xi_n$ and α, γ and m are suitable constants. This form is very close to a common random number generator $I_{n+1} = (\alpha I_n + \gamma) \pmod{m}$ [15]. An interesting question raised by this similarity, one that we leave open, is whether there is a deterministic fractal whose counting staircase generates an acceptable pseudo-random sequence.

EPAPS AUXILIARY MATERIAL: DATA

ANALYSIS OF DRIP PAINTINGS

Notes: Results obtained using the Photoshop colour separation method are marked PS; using adaptive RGB mesh, marked RGB. Known Pollock works are identified by name and their serial number in *Jackson Pollock: A Catalogue Raisonné of Paintings, Drawings and Other Works* by F.V. O'Connor and E.V. Thaw (Yale University Press, New Haven, 1978), hereafter abbreviated JPCR. For some paintings the digital image was cropped slightly before analysis. In these cases we give the dimensions of the cropped image used in each analysis. For layers that were force fit the results are marked ff; see below for a precise description of force-fitting. The quantity that is directly inferred from the data is $\ln L_T$ but we present L_T values since it is more easy to visualise. However it should be kept in mind that by exponentiating the measured quantity we are amplifying the errors. Thus our two methods agree much better on the location of the box-counting transition than this tabulation of L_T values may suggest. For each painting the results are briefly summarised at the end.

Force-fitting: Ref [7] describes a more relaxed procedure called force-fitting that can be applied to paintings that fail to pass the strict authentication test. Force-fitting imposes the constraint that $L_T > 1.0$ cm, thereby automatically satisfying authentication criterion (2). Thus authentication is reduced to checking that the other criteria are fulfilled.

1. Untitled 1: (Poured media on board). Matter painting that resembles Pollock's *Free Form*.

Physical Dimensions: 35.6×44.5 cm
Digital Image: 2020×2520 (PS black) 1994×2487 (PS white) 1986×2502 (RGB)
Range of box sizes: 0.2 cm to 3.1 cm (PS) 0.2 cm to 3.1 cm (RGB)

Black Layer:
Area of layer: 43.0 % (PS) 38.46 % (RGB)
Noise: 0.023 (PS) 0.017 (RGB) 0.020 (RGB ff)
L_T: 1.0 cm (PS) 0.8 cm (RGB) 1.0 cm (RGB ff)
Lower dimension: 1.41 (PS) 1.71 (RGB) 1.73 (RGB ff)
Upper dimension: 1.98 (PS) 1.98 (RGB) 2.00 (RGB ff)

White Layer:
Area of Layer: 13.9 % (PS) 10.86 % (RGB)
Noise: 0.024 (PS) 0.023 (RGB) 0.025 (PS ff) 0.024 (RGB ff)
L_T: 0.85 cm (PS) 0.95 cm (RGB) 1.0 cm (PS ff) 1.0 cm (RGB ff)
Lower dimension: 1.47 (PS) 1.35 (RGB) 1.49 (PS ff) 1.36 (RGB ff)
Upper dimension: 1.97 (PS) 1.93 (RGB) 2.00 (PS ff) 1.95 (RGB ff)

Composite Layer:
Noise: 0.018 (PS) 0.017 (RGB) 0.021 (PS ff) 0.021 (RGB ff)
L_T: 0.58 cm (PS) 0.59 cm (RGB) 1.0 cm (PS ff) 1.0 cm (RGB ff)
Lower Dimension: 1.86 (PS) 1.82 (RGB) 1.90 (PS ff) 1.86 (RGB ff)
Upper Dimension: 2.02 (PS) 2.02 (RGB) 2.07 (PS ff) 2.04 (RGB ff)

RGB Colour partition:

White = 111, 010
Black = 001, 011, 101,
00-00-01, 00-01-00, 00-01-01,
000-000-000, 000-000-001, 000-001-000, 000-001-001
Brown = 100, 110,
01-00-00, 01-00-01, 01-01-00, 01-01-01,
001-000-000, 001-000-001, 001-001-000, 001-001-001

Summary: Satisfies fractal authentication criteria if the more lax force-fitting procedure is allowed.

2. Untitled 14: (Poured media on board). Matter painting that resembles Pollock's *Wooden Horse.*

Physical Dimensions: 31.7 cm × 46.4 cm.
Digital Image: 1764 × 2568 pixels
Range of box sizes: 0.2 cm to 3.1 cm (PS)

Red Layer:
Area of Layer: 10.0 % (PS)
Noise: 0.014 (PS)
L_T : 1.4 cm (PS)
Lower Dimension: 1.36 (PS)
Upper Dimension: 1.69 (PS)

Orange Layer:
Area of Layer: 1.7 % (PS)
Noise: 0.024 (PS)
L_T : 0.5 cm (PS)
Lower Dimension: 1.28 (PS)
Upper Dimension: 0.91 (PS)

Yellow Layer:
Area of Layer: 5.1 % (PS)
Noise: 0.018 (PS)
L_T : 1.2 cm (PS)
Lower Dimension: 1.08 (PS)
Upper Dimension: 1.69 (PS)

Blue Layer:
Area of Layer: 4.2 % (PS)
Noise: 0.023 (PS)
L_T : 1.0 cm (PS)
Lower Dimension: 1.05 (PS)
Upper Dimension: 1.67 (PS)

Black Layer:
Area of Layer: 11.6 % (PS)
Noise: 0.014 (PS)
L_T : 1.2 cm (PS)
Lower Dimension: 1.36 (PS)
Upper Dimension: 1.71 (PS)

White Layer:
Area of Layer: 11.0 % (PS)
Noise: 0.010 (PS)
L_T : 2.0 cm (PS)
Lower Dimension: 2.02 (PS)
Upper Dimension: 1.81 (PS)

Summary: Does not satisfy fractal authentication criteria. Exhibits anomalous dimensions in orange and white layers.

3. Free-Form Pollock (1946) [JPCR 165] (Oil on canvas).

Physical Dimensions: 48.9 cm × 35.5 cm
Digital Image: 4550 × 3253 (PS Black), 4576 × 3288 (PS White); 2277 × 1629 pixels (RGB)
Range of box sizes: 0.1 cm to 4.5 cm (PS) 0.2 cm to 4.2 cm (RGB)

NB: the image was coarsened before RGB analysis to speed up computations. In principle this should have no effect on the fractal analysis since the smallest box sizes exceed the coarsening scale. This expectation is borne out by the concordance between the PS and RGB results.

Black Layer:
Area of Layer: 56.0 % (PS) 54.39 % (RGB)
Noise: 0.015 (PS) 0.013 (RGB)
L_T: 1.0 cm (PS) 1.0 cm (RGB)
Lower dimension: 1.79 (PS) 1.85 (RGB)
Upper dimension: 2.05 (PS) 2.02 (RGB)

White Layer:
Area of Layer: 20.7 % (PS) 23.48 % (RGB)
Noise: 0.019 (PS) 0.019 (RGB) 0.021 (PS ff)
L_T: 0.9 cm (PS) 1.0 cm (RGB) 1.0 cm (PS ff)
Lower dimension: 1.57 (PS) 1.60 (RGB) 1.58 (PS ff)
Upper dimension: 2.04 (PS) 2.00 (RGB) 2.06 (PS ff)

Composite Layer:
Noise: 0.013 (PS) 0.012 (RGB) 0.012 (RGB ff) 0.015 (PS ff)
L_T: 0.8 cm (PS) 0.65 cm (RGB) 1.2 cm (RGB ff) 1.1 cm (PS ff)
Lower dimension: 1.93 (PS) 1.94 (RGB) 1.96 (RGB ff) 1.93 (PS ff)
Upper dimension: 2.06 (PS) 2.01 (RGB) 2.02 (RGB ff) 2.075 (PS ff)

RGB Colour partition:
Black = 000, 001, 011, 101
Red = 100
White = 010, 110, 111

Summary: Satisfies fractal authentication criteria if the more lax force-fitting procedure is allowed.

4. The Wooden Horse: Number 10A, 1948 Pollock (1948) [JPCR 207] (Oil and enamel paint on canvas).

Physical Dimensions: 90.1 × 190.5 cm
Digital Image: 2340 × 1176 (PS and RGB)
Range of Box Sizes: 0.8 cm to 14.2 cm (PS) 0.8 cm to 14.0 cm (RGB) 0.8 cm to 9.5 cm (RGB, Orange Layer)

Red Layer:
Area of Layer: 3.6 % (PS) 2.5 % (RGB)
Noise: 0.023 (PS) 0.026 (RGB)
L_T: 4.32 cm (PS) 4.32 cm (RGB)
Lower dimension: 1.16 (PS) 1.12 (RGB)
Upper dimension: 1.56 (PS) 1.63 (RGB)

Orange Layer:
Area of Layer: 1.7 % (PS) 1.9 % (RGB)
Noise: 0.0301 (PS) 0.027 (RGB)
L_T: 3.23 cm (PS) 2.67 cm (RGB)
Lower dimension: 1.39 (PS) 1.50 (RGB)

Upper dimension: 1.18 (PS) 1.25 (RGB)

Yellow Layer:
Area of Layer: 1.2 % (PS) 1.3 % (RGB)
Noise: 0.026 (PS) 0.018 (RGB)
L_T: 7.63 cm (PS) 1.67 (RGB)
Lower dimension: 1.11 (PS) 1.26 (RGB)
Upper dimension: 1.05 (PS) 1.08 (RGB)

Black and Blue Layers:
Area of Layer: 10.3 % (PS) 2.3 % (Blue, RGB) 7.4 % (Black, RGB)
Noise: 0.028 (PS) 0.024 (Black RGB) 0.025 (Blue RGB)
L_T: 3.91 cm (PS) 4.32 cm (Black RGB) 4.32 cm (Blue RGB)
Lower dimension: 1.44 (PS) 1.35 (Black RGB) 1.14 (Blue RGB)
Upper dimension: 1.92 (PS) 1.79 (Black RGB) 1.73 (Blue RGB)

White Layer:
Area of layer: 5.5 % (PS) 9.1 %
Noise: 0.031 (PS) 0.026 (PS; trimmed range) 0.026 (RGB)
L_T : 3.91 cm (PS) 3.91 cm (RGB)
Lower dimension: 1.30 (PS) 1.39 (RGB)
Upper dimension: 1.82 (PS) 1.86 (RGB)

RGB Colour Partition:

Blue = 001, 011,
00-00-01, 00-01-01, 01-00-01,
010-010-011, 010-011-010, 010-011-011, 011-010-011, 011-011-011
0100-0100-0101, 0100-0101-0101, 0101-0100-0101
black = 010,
00-00-00, 00-01-00, 01-00-00,
010-010-001
0100-0100-0100, 0100-0101-0100, 0101-0100-0100, 0101-0101-0100,
0101-0101-0101
Red = 101,
10-00-00, 10-00-01, 10-01-00, 11-00-00, 11-01-00, 11-01-01
111-100-011
White = 111
Brown = 10-01-01, 10-10-01
011-010-001, 011-011-001
011-010-010, 011-011-010
110-100-010, 110-100-011,
Yellow and orange = 10-10-00, 11-10-00, 11-11-00, 11-11-01
110-101-010, 110-101-011, 111-100-010, 111-101-010, 111-101-011

Notes: In the PS analysis the blue and black layers were analysed as a composite. In the RGB analysis the horse's head was not fully excluded from the white layer; thus the PS analysis of the white layer is more accurate. The yellow and orange layers in the RGB analysis were separated by incorporating spatial information. If the pixels lay in the appropriate region of RGB and real space they were deemed yellow; otherwise orange.

Summary: Does not satisfy fractal authentication criteria. Exhibits anomalous dimensions in the orange and yellow layers.

5. Untitled: Pollock (1950) [JPCR 797] (Enamel on paper).

Physical Dimensions: 28.3 cm × 150.3 cm
Digital Images: 1145 × 5150 pixels (PS and RGB) 1145 × 2908 (RGB - cropped).

Range of box sizes: 0.1 cm to 2.7 cm (PS) 0.1 cm to 4.4 cm (RGB) 0.1 cm to 3.0 cm (RGB - cropped)

Black Layer:
Area of Layer: 5 % (PS) 5 % (RGB)
Noise: 0.020 (PS) 0.024 (RGB) 0.024 (RGB - cropped)
L_T: 0.5 cm (PS) 0.5 cm (RGB) 0.5 cm (RGB - cropped)
Lower dimension: 1.73 (PS) 1.72 (RGB) 1.72 (RGB - cropped)
Upper dimension: 1.36 (PS) 1.37 (RGB) 1.39 (RGB - cropped)

RGB Colour partition:
Black = 000

Summary: Does not satisfy fractal authentication criteria. Exhibits anomalous dimensions.

6. Number 8, 2007: Ash and Hallen (2007) (Oil on canvas).

Physical Dimensions: 122 cm × 152 cm (approx)
Digital Image: 1387 × 1668 pixels (PS) 1192 × 1566 pixels (RGB)
Range of box sizes: 0.9 cm to 15.3 cm (PS) 0.3 cm to 6.0 cm (RGB)

Black Layer:
Area of Layer: 44.0 % (PS) 58.3 % (RGB)
Noise: 0.014 (PS) 0.022 (RGB)
L_T: 3.8 cm (PS) 1.6 cm (RGB)
Lower dimension: 1.89 (PS) 1.81 (RGB)
Upper dimension: 2.08 (PS) 2.05 (RGB)

RGB Colour partition:
Black = 000, 001, 010, 011, 100, 101, 110
Background = 111

Comments: The discrepancy between the percentage area of black obtained by the two colour separation methods is is due to the different way the painting was cropped before colour separation. The cropped image used in the Photoshop analysis contained a margin that was largely white. The discrepancy between the L_T values is presumably due to the same cause.

Summary: Satisfies fractal authentication criteria.

7. Composition with Red and Black: Ash and Hallen (2007) (Oil on canvas).

Physical Dimensions: 122 cm × 152 cm (approx)
Digital Image: 1288 × 1536 pixels
Range of box sizes: (PS) 0.3 cm to 16.4 cm (RGB)

Black Layer:
Area of Layer: 33.4 % (PS) 37.2 % (RGB)
Noise: 0.023 (PS) 0.021 (RGB)
L_T: 1.75 cm (PS) 1.75 cm (RGB)
Lower dimension: 1.68 (PS) 1.64 (RGB)
Upper dimension: 2.02 (PS) 2.01 (RGB)

Red Layer:
Area of Layer: 17.0 % (PS) 22.3 % (RGB)
Noise: 0.020 (PS) 0.025 (RGB)
L_T: 4.13 cm (PS) 1.59 cm (RGB)
Lower dimension: 1.48 (PS) 1.48 (RGB)
Upper dimension: 2.01 (PS) 1.98 (RGB)

RGB Colour partition:
Black = 001, 010, 011,
00-00-00, 00-00-01, 00-01-00, 00-01-01, 01-01-00, 01-01-01

Red = 100, 101, 110,
01-00-00, 01-00-01
Background = 111

Summary: Satisfies fractal authentication criteria.

Figure1. Pollock Paintings top: *The Wooden Horse: Number 10A, 1948* (1948); bottom: *Free Form* (1946) . Both paintings undisputedly by Pollock; *The Wooden Horse: Number 10A, 1948* fails to satisfy the fractal authentication criteria for Pollock paintings; *Free Form* meets the criteria when subject to force fitting. Both paintings oil and/or enamel on canvas. (Paintings to appear after publication.)
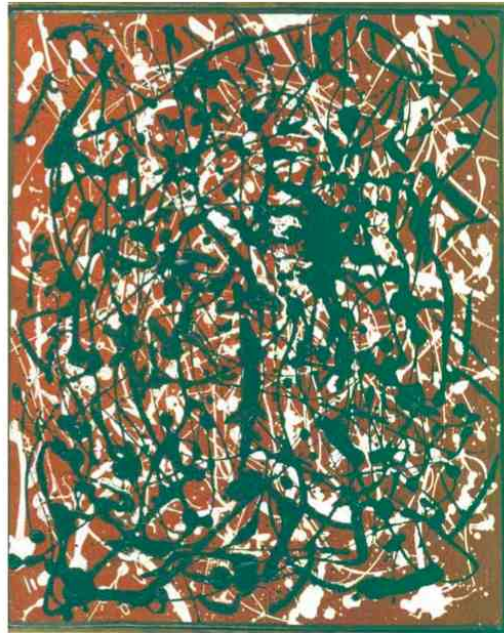
Figure 2. Matter Paintings The Matter paintings that resemble Pollock's *Wooden Horse: Number 10A, 1948* (top) and *Free Form* (bottom). *Untitled 14* (top) fails the authentication criteria in the same manner as *Wooden Horse: Number 10A, 1948*; *Untitled 1* (bottom) meets the criteria to the same extent as *Free Form*. Both paintings poured media on board.

Figure 3. Paintings by Ash and Hallen. *Number 8,2007* (2007) (top left) ; *Composition with Red and Black* (2007) (top right); detail from *Untitled* (2007) (bottom). Three paintings from a series of nine, two of which (*Number 8,2007* and *Composition with Red and Black*) have been been analysed and found to satisfy the fractal authentication criteria used to identify Pollock paintings. All paintings oil on canvas.
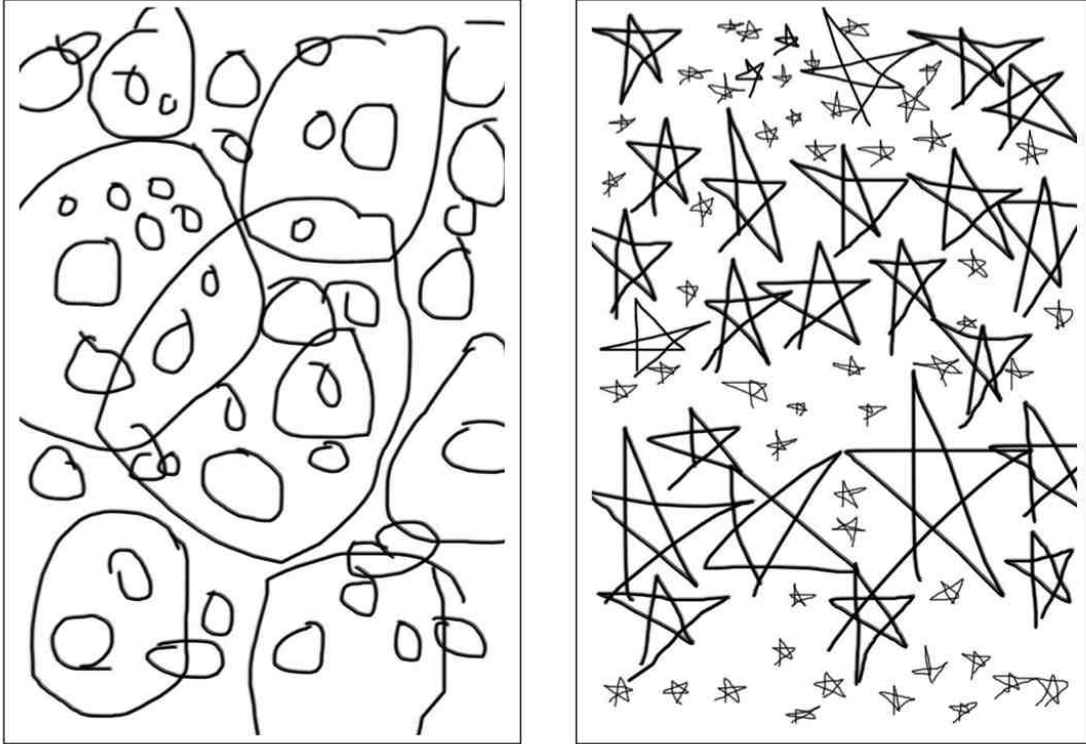
Figure 4. Sketches *Gross Pebbles* (left) and *Mixed Stars* (right) by Katherine Jones-Smith (2006). Like *Untitled 5* ref (7), these crude drawings satisfy the fractal authentication criteria used to identify Pollock, although they are indisputably not works by Pollock. These freehand drawings were created using Adobe Photoshop as described in ref (7).